WATER RESOURCES RESEARCH, VOL. 49, 7887–7899, doi:10.1002/2013WR013762, 2013

The impact of floods on infiltration rates in a disconnected stream

Wenfu Chen,[1] Chihchao Huang,[2] Minhsiang Chang,[3] Pingyu Chang,[4] and Hsuehyu Lu[5]

Received 1 March 2013; revised 31 October 2013; accepted 4 November 2013; published 3 December 2013.

[1] A few studies suggest that infiltration rates within streambeds increase during the flood season due to an increase in the stream stage and the remove of the clogged streambed. However, some studies suggest that a new clogging layer will quickly form after an older one has been eroded, and that an increase in water depth will compress the clogging layer, making it less permeable during a flood event. The purpose of this work was to understand the impact of floods on infiltration rates within a disconnected stream. We utilized pressure data and daily streambed infiltration rates determined from diurnal temperature time series within a streambed over a period of 167 days for five flood events. Our data did not support the theory that floods linearly increase the infiltration rate. Since the streambed was clogged very quickly with a large load of suspended particles and compaction of the clogged layer, infiltration rates were also low during the flooding season. However, due to an increase in the wet perimeter within the stream during flooding periods, the total recharge amount to the aquifer was increased.

Citation: Chen, W., C. Huang, M. Chang, P. Chang, and H. Lu (2013), The impact of floods on infiltration rates in a disconnected stream, *Water Resour. Res.*, *49*, 7887–7899, doi:10.1002/2013WR013762.

1. Introduction

[2] Interactions between ground and surface water are important for the effective management of water resources. Based on interactions, streams are conceptually classified as gaining, losing, or disconnected [*Sophocleous*, 2002; *Brunner et al*., 2011]. In a disconnected stream, an unsaturated zone exists between the streambed and the water table. An unsaturated zone generally develops while the streambed is clogged and its hydraulic conductivity is less than the underlying aquifer, with a ratio of 0.1 to 0.01 [*Su et al*., 2007; *Brunner et al*., 2009]. The infiltration flux of a disconnected stream is higher than the condition of the connection that has been referred to as the "maximum losing condition," a further decrease in the groundwater table that does not impact the infiltration rate [*Moore and Jenkins*, 1966; *Peterson et al*., 1984; *Osman and Bruen*, 2002; *Desilets et al*., 2008; *Parsons et al*., 2008; *Brunner et al*., 2009, 2011; *Irvine et al*., 2012].

[3] Infiltration rates of a disconnected stream are controlled by the hydraulic properties of the aquifer, the clogging layer, and the stream water level. Infiltration rates decrease with a fine grain layer deposited on the streambed, and/or the streambed is clogged by filling its void. *Hatch et al*. [2010] discussed the spatial and temporal variations for stream discharge, sediment load, and streambed hydraulic properties and found that the streambed hydraulic conductivity varied between 10^{-6} and 10^{-4} m/s, and tended to decrease (by an order of magnitude or more) as sediment was deposited on the streambed during low flow conditions. As indicated by Darcy's law, infiltration rates increase linearly with river water depth while the hydraulic conductivity remains constant [*McDonald and Harbaugh*, 1996; *Shanafield et al*., 2012].

[4] Some studies suggest that infiltration rates in streambeds increase during the flood season due to the increase of the stream stage and the removal of the clogged streambed. For example, during summer flood months, the average infiltration rate doubled as compared to that during winter within the Rio Puerco stream [*Heath*, 1983]. *Vazquez-Sune et al*. [2007] indicated that the infiltration rate of the disconnected stream dramatically increased during the flood period and estimated that 40% of total aquifer (Lower Llobregat, Spain) inputs arose from river flooding infiltration. The authors proposed that the clogged layer may be fully removed by flood waters and an increase in the wet perimeter and the riverhead. *Doble et al*. [2012] suggested that flooding events have two processes that are referred to as scour and fill. The preferential entrainment of fine sediment during a flood's scour leads to overall bed coarsening and to an increase in vertical hydraulic conductivity and infiltration fluxes [*Simpson and Meixner*, 2012].

[5] However, by quickly forming a new clogging layer within the streambed and due to compression of the clogged streambed during the flood season, as observed in practice field cases and column tests, some researchers have suggested that infiltration rates do not increase [*Bouwer and Rice*, 1989; *Houston et al*., 1999; *Pavelic et al*., 2011].

[1]Institute of Hot Spring Industry, Chia Nan University of Pharmacy and Science, Tainan, Taiwan, ROC.
[2]Department of Resources Engineering, National Chen-Kung University, Tainan, Taiwan, ROC.
[3]Central Geological Survey, Taipei, Taiwan, ROC.
[4]Institute of Applied Geosciences, National Taiwan Ocean University, Keelung, Taiwan, ROC.
[5]Department of Earth and Environmental Sciences, National Chung Cheng University, Min-Hsiung, Chia-Yi, Taiwan, ROC.

Corresponding author: W. Chen, Institute of Hot Spring Industry, Chia Nan University of Pharmacy and Science, Tainan, Taiwan, ROC. (chenwenfu@mail.chna.edu.tw)

0043-1397/13/10.1002/2013WR013762

Major factors influencing the clogging process are the size distribution of the streambed and the suspended load, the concentration of the suspended load, and the velocity of infiltration [*Behnke*, 1969; *Schalchli*, 1992, 1995; *Lentz and Freeborn*, 2007]. During a flood event, an older clogged streambed may be eroded. However, a new one will quickly be formed while the concentration of the suspended load is very high [*Gibson et al*., 2011]. An increase in water depth compresses the clogging layer, making it less permeable [*Bouwer*, 2002]. A study of the Kuiseb River in Namibia found that all floods produced very similar flux rates, suggesting that recharge rates are less impacted by flood stages [*Dahan et al*., 2008].

[6] The purpose of this work was to understand the impact of flooding effects on infiltration rates within a disconnected stream. We sought to understand whether or not infiltration rates increased during flood events. We employed diurnal temperature time series in order to determine daily streambed infiltration rates during several flood events in the Chohsui Stream of central Taiwan. Our data does not support the theory that floods linearly increase infiltration.

2. The Hydrogeology of the Field Site

[7] The Chohsui Stream in central Taiwan is a perennial stream that flows westward from an altitude of 100 meters beside a mountain front and deposits an alluvial (fluvial) fan, spanning an area of approximately 40 × 50 km^2, on the coastal plain (Figure 1a). The mountains rise up to over 3000 m within a short distance of 60 km. Due to erosion, the high and steep mountain drainage basin produces a wide range of flood discharge and sediments. The discharge of water in the upper fan varies over several orders of magnitude; for example, at our study site, 13 m^3/s during the dry season and 1300 m^3/s during a typhoon flood in 2011. Suspended loads within the stream varied as well, by approximately <1.0 g/L for lower water depths (< 50 cm) and higher to over 5.0 g/L for a 250 cm water depth during floods (Figure 2).

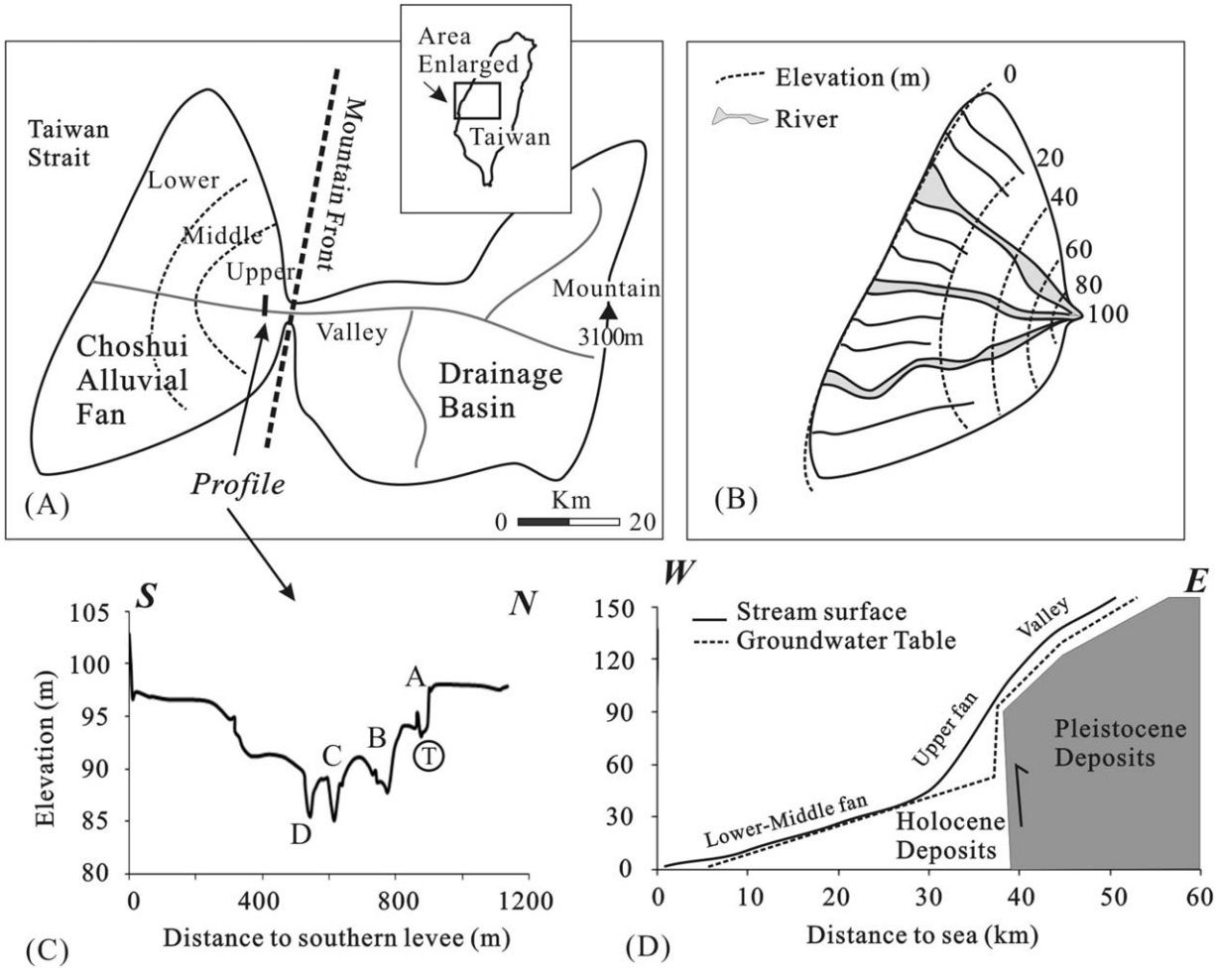

Figure 1. (a) The location of the Choshui Alluvial Fan, central Taiwan. The stream flows westward to the Taiwan Strait. (b) The river systems and the elevation within the Choshui Fan. (c) The streambed elevation profile with a south to north direction. The four active channels within the Choshui Stream are denoted as A to D. Our test site was located in Channel A ("T" in a circle). (d) The longitudinal elevation profile and the groundwater table.

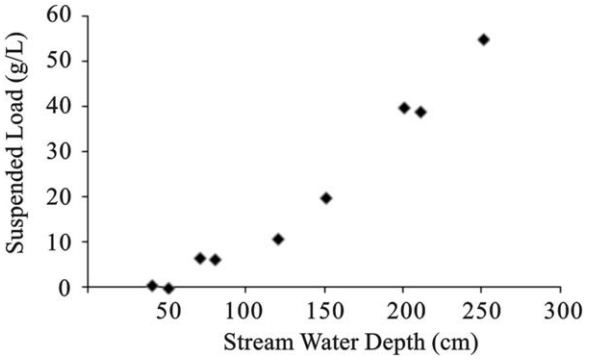

Figure 2. Suspended load increases as the stream water depth increases within the Choshui Stream.

[8] From 1697 to present, at least three river systems developed and formed a fan shape (Figure 1b). The main discharged river moved north in 1697, south in 1793, and back to north in 1898, generally with large destruction to human settlements. In 1911, the main course of the river was constrained by levees to the present central position of the fan [*Chang*, 1983]. The upper fan of the Choshui Stream's main course consists of four active channels during the lower discharge season with a sandy gravel streambed and a slope of 6.4×10^{-3}. Our study site was located in channel A (Figure 1c).

[9] The grain size distribution of the streambed material is composed mainly of sand (33%) and gravel (65%), with silt and clay contributing less than 2% (Figure 3a). The porosity of the streambed material, as measured by the laboratory, was approximately 0.25–0.45 depending on the compaction of the samples and their preparation. The gravel was mainly composed of quartzite and metasandstone (72%) with a minor portion of slate (28%). However, slate represented the major proportion of sand with a percentage of approximately 59%. Figure 3b provides a lab-measured retention curve for a typical streambed at our study site. The streambed was sand dominated with lower values for the water-entry value and the air-entry value than for high silt and clay content soils.

[10] The unconfined aquifer underneath the streambed has a thickness of over 300 m and is composed of gravel and sand layers with sediments that range in age from the Pleistocene to the present (Figure 1d). According to nearby monitoring wells, the groundwater table at the upper fan is located approximately 30–40 m beneath the ground's surface [*Central Geological Survey*, 1999; *Chen and Liu*, 2003, 2005]. Streams in the upper fan are classified as disconnected streams because a massive unsaturated zone occurs beneath the streambed. The groundwater tables are shallow, 0–3 m beneath streams in the mountain valley and in the middle fan these sections of streams are identified as a gaining reach during the flood season and as a losing reach during the dry season (Figure 1d).

3. Research Method

[11] Among the many methods for determining the streambed infiltration rate—water budgets, seepage meters, base flow discharges, heat tracers, isotopic tracers, etc.—the heat tracer of diurnal temperature time series in the streambed is one of the most frequently used methods [*Scanlon et al*., 2002; *Stonestrom and Blasch*, 2003; *Stonestrom and Constantz*, 2003; *Anderson*, 2005; *Constantz*, 2008]. At least two temperature logs should be installed, one in the streambed (not deeper than 100 cm in depth), and the other at the streambed surface. Downward heat transfer from the surface to the deeper part of the streambed occurs by conduction and advection for stream water percolating. The amplitude of the diurnal temperature time series in the streambed is smaller than that on the streambed surface and has a phase shift. Using the difference in temperature amplitude (ΔA) and phase shift ($\Delta\Phi$) in the following vertical flow equation, we were able to calculate the infiltration rate based on one-dimensional heat transfer:

$$(\kappa/\rho C)(\partial^2 T/\partial Z^2) - q(\rho_w C_w/\rho C)(\partial T/\partial Z) = \partial T/\partial t \qquad (1)$$

[12] The first term on the left-hand side of the equation represents heat conduction; κ is the thermal conductivity (W/m°C) of bulk streambed sediments; ρ and C are the density (kg/m^3) and the specific heat (J/kg°C) of the sediments according to the water content; T is the temperature (°C); and Z is the depth (m). The second term on the left-hand side of the equation is an advection term, where q is the infiltration rate (m/s) that is equal to the product of the streambed percolation velocity (m/s) and the water content

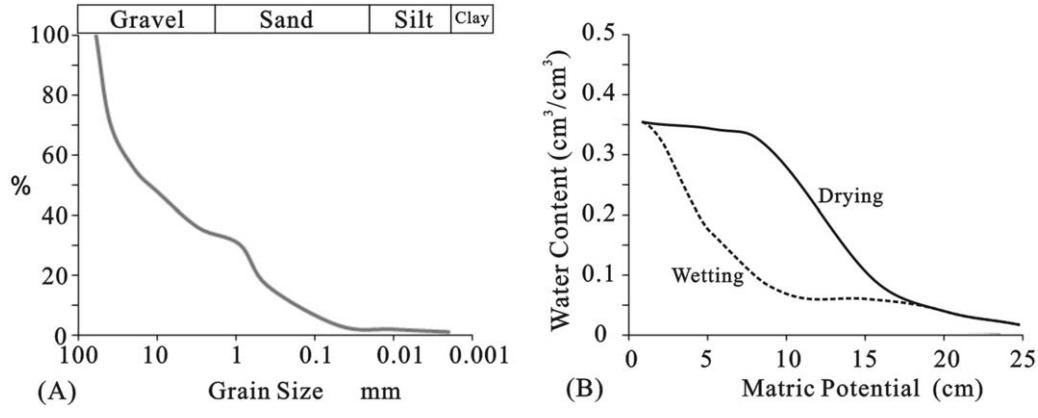

Figure 3. The grain size distribution (a) and the retention curve (b) of the study's streambed material.

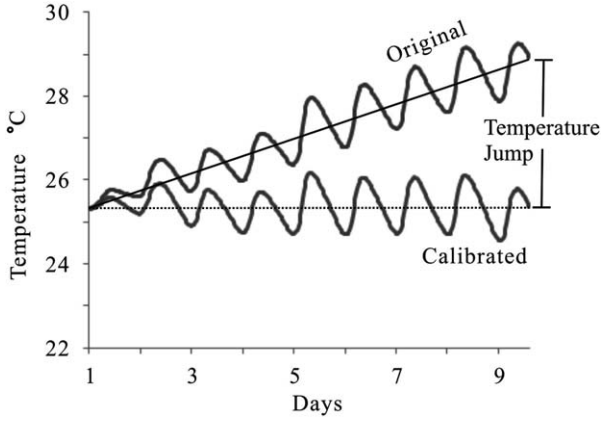

Figure 4. The temperature time series for several days for a field site tends toward an increasing or decreasing trend, displayed as a temperature jump, while the data are discretized and simulated by the diurnal data set.

of the sediments; and ρ_w and C_w are the density and the specific heat of the water. On the right-hand side of the equation, t is the time (s) [*Suzuki*, 1960; Stallman, 1965; *Constantz*, 2008]. For the unsaturated condition, the thermal conductivity, the density, and the specific heat of the bulk streambed material are varied due to water content.

[13] To solve equation (1), we developed two computer programs. One of the programs determined the thermal conductivity of the streambed using two time series of temperature data when no percolation occurred. The proposed model had two unknowns, one for the initial temperature and one for the temperature of the lower boundary. We initially assumed 25°C for all of the spatial nodes in the model and "initial temperatures" were generated for a period of 5 days in the program before they came into equilibrium with the model boundary temperatures [*Niswonger and Prudic*, 2003]. The lower boundary temperature was also determined, while the program performed the best fitting procedure for thermal diffusivity.

[14] The second program determined the streambed percolation velocity using two time series of temperature data and known parameters for thermal conductivity, density, specific heat, and the water content of the streambed. The calculation was based on a diurnal period; that is, if there were 6 days of data, six values for the percolation velocity were determined.

[15] The temperature time series for several days at a field site generally tended towards an increasing or decreasing trend that displayed a temperature jump, whereas the data were discretized and simulated by the diurnal data set (Figure 4). Our study suggested preprocessing these data sets using a linear transform in order to eliminate the temperature jump [*Hatch et al*., 2006]. For example, one data set with a temperature jump of 0.5°C had a calculated thermal diffusivity of 6.45×10^{-7} m^2/s with a difference of 5.7×10^{-6}°C between the simulated and measured amplitude, and with an obvious time shift. After calibrating the data set, the calculated thermal diffusivity was approximately 7.3×10^{-7} m^2/s and the amplitude difference was less than 3.6×10^{-6}°C with no time shift between the simulated and the measured temperature series.

[16] To verify our programs, we tested the following data sets (Table 1): (1) A case study by *Tsai et al*. [2008] that determined that the thermal diffusivity of the soil was approximately 6.23×10^{-7} m^2/s. The temperature in a 1 m depth was approximately 25.5°C. We calculated an approximate value of 6.51×10^{-7} m^2/s for the thermal diffusivity and 25.80°C for the lower boundary temperature using the same temperature series data set (October 1998). (2) The case study by *Munz et al*. [2011] who reported an analytical thermal diffusivity of approximately 11.9×10^{-7} m^2/s for a quartz sand layer (June–October 2010) and, using our program, obtained an approximate value of 14.5×10^{-7} m^2/s. (3) *Ronan et al*. [1998] in their study of the Vicee Canyon (Nevada, US), using the VS2DH numerical model, reported a streambed with a thermal diffusivity of 8.7×10^{-7} m^2/s and a calculated streambed percolation velocity of 1.38×10^{-5} m/s. We used a temperature data set from 24 May 1994 and calculated a percolation velocity of 1.89×10^{-5} m/s identical to the measured value. (4) In the River Tern (location T1) of Shropshire UK, *Keery et al*. [2007] obtained streambed percolation velocities of 2.9–6.4×10^{-6} m/s using the analytical method. Using the same temperature data (8 July 2005), we calculated a percolation velocity of approximately 6.79×10^{-6} m/s. (5) A study in Juday Creek (Indiana, US) by *Silliman and Booth* [1993] and *Silliman et al*. [1995] who reported analytical values for the percolation velocity of 8.3×10^{-8} m/s – 8.3×10^{-7} m/s (15 August 1991). Our program calculated a value of 7.91×10^{-7} m/s.

[17] Temperature and pressure data were collected using automatic probes (Schlumberger Mini-Diver) over half-hour intervals. The probe's working range was 0–80°C and had an accuracy of ±0.1°C, a resolution of 0.01°C, and a working range for pressure up to 10 mH_2O with an accuracy of ± 0.01 mH_2O and a resolution of 0.002 mH_2O. The

Table 1. The Numerical Solution Verification of Our Program

			Low Boundary Temperature (°C)	
Data Sources	From References	Our Program	From References	Our Program
Thermal Diffusivity (m^2/s)				
Tsai et al. [2008]	6.23×10^{-7}	6.51×10^{-7}	25.5	25.8
Munz et al. [2011]	11.9×10^{-7}	14.5×10^{-7}	[a]	21.19
Percolation Velocity (m/s)				
Ronan et al. [1998]	1.38×10^{-5}	1.89×10^{-5}	12–13	12.5
Keery et al. [2007]	$2.9–6.4\times10^{-6}$	6.79×10^{-6}	[a]	6.0
Silliman et al. [1995]	$8.3–83\times10^{-7}$	7.91×10^{-7}	[a]	20.0

[a]Not available in references.

probe's dimensions were 9 cm in length and 2.2 cm in diameter. To obtain a better resolution, to consider vertical heat transfer, and to avoid crossing many sediment layers that would lead to a decrease in accuracy, probes were buried horizontally within the streambed.

[18] An unsaturated zone that developed in the streambed was noted when the pressure in the streambed was equal to or less than the ambient air pressure [*Massmann and Farrier*, 1992; *Neeper*, 2002]. The vertical hydraulic gradient (I) between two points in the streambed was determined by the pressure difference and the distance between two points for the saturated condition (the pressure in the streambed was larger than the air pressure), as follows:

$$I=(P_0-P_1+L)/L \quad (2)$$

where P_0 is the pressure of the upper point, P_1 is the pressure of the lower point, and L is the separation distance. The percolation velocity (v) was determined by the T_0/T_1 diurnal temperatures. T_0 is the temperature series for the upper point and T_1 is the temperature series for the lower point. The vertical hydraulic conductivity (K) between the two points was derived using Darcy's law, as follows:

$$K=v/I \quad (3)$$

[19] For collecting data for erosion/deposition in a streambed, each buried probe was taped with a scale wire in order to begin checking the buried depth, and was manually recorded each day.

4. Thermal Parameters

[20] The uncertainty associated with the streambed infiltration estimation was dependent on the accuracy of the thermal conductivity, the heat capacity (or specific heat) and the experimental design (separation distance) [*Hatch et al*., 2006; *Shanafield et al*., 2011; *Soto-Lopez et al*., 2011]. The thermal conductivities of the streambed material were measured in the laboratory using a polyethylene circular cylinder (with a diameter of 40 cm) with an outer insulation layer of polyethylene foam (with a thermal conductivity of 0.032 W/m°C). Thermal diffusivities were determined using a diurnal temperature time series and the known density and specific heat. The thermal diffusivities of our streambed samples (saturated at 0.35 porosity) were $6.0–7.2\times10^{-7}$ m^2/s with an average of 6.6×10^{-7} m^2/s, which was approximately 1.94 W/m°C for the thermal conductivity. The thermal diffusivities of dry streambed samples were $2.1–2.6\times10^{-7}$ m^2/s with an average of 2.3×10^{-7} m^2/s; and the thermal conductivity was 0.33 W/m°C (Table 2).

[21] The specific heat of the gravel samples was measured using a calorimetric method [*Kukkonen et al*., 2011]. The sample was heated to approximately 98.5°C in a hot bath then placed into a calorimeter containing a known (by mass) amount of water. The final equilibrium temperature of the calorimeter-water-sample system was measured. The specific heat was calculated based on the initial and final temperatures of the sample and the calorimeter, the heat capacity of the calorimeter, and the masses of the water and the sample. Based on the porosity (0.35) and the lithology percentage, the specific heat of the saturated streambed material was approximately 1.45 kJ/kg°C, on average, while the value was approximately 0.85 kJ/kg°C for the dry condition (Table 2).

[22] The unsaturated thermal conductivities were assumed based on the water content and the values of the saturated or dry condition. We assumed that the relationship was linear, as follows: for a water content of 0.25, 0.15, and 0.05, the values of the interpolation for the thermal conductivities were 1.54, 1.13, and 0.73 W/m°C, respectively (Table 3). The values of the density and the specific heat for the streambed material for various water contents were estimated using the linear interpolation of dry and saturated values.

[23] Silt fills the pores of the streambed to form a clogging layer that also changes the thermal properties. We suggest that the thermal properties can be estimated by assuming the percentage of silt fill (e.g., 10% and 20% of bulk volume (Table 4)). The density and specific heat of the clogging layer were estimated using the percentage of solid and water. Thermal conductivity was determined using a linear interpolation provided by a preclogged streambed and slate or quartzite. The clogging layer at our study site was only a few centimeters in thickness. Using the thermal properties provided in Table 4, we assumed a clogging layer of 10 cm in thickness and determined that the errors were within 10%, not a level that would significantly impact our results.

[24] Errors in the infiltration rate for a saturated streambed mainly resulted from uncertainties in sensor spacing, porosity, thermal diffusivity, and temperature sensor accuracy [*Shanafield et al*., 2011; *Soto-Lopez et al*., 2011]. Data for a saturated condition in Test 3, 7–25 October, were used to evaluate the errors induced by those uncertainties. Sensor spacing and its uncertainty were 7 ± 1 cm, the porosity was 0.35 ± 0.05, and thermal diffusivity was $6.6\pm1.0\times10^{-7}$ m^2/s. The diurnal amplitude of the temperature was 1–7°C with a sensor accuracy of ±0.1°C. Errors due to porosity and thermal diffusivity uncertainty were less than 20%, and less than 40% due to sensor spacing and temperature sensor accuracy (Figure 5).

5. Results

5.1. Clogging During Flood Events

[25] A summary of the total of the three tests, Tests 1–3, from 25 July to 19 December 2011 is shown in Table 5. The initial depths of probes were 0 and 50 cm for Tests 1 and 2 (two probes); and 0 cm, 7 cm, and 50 cm (three probes) for Test 3. The P07 Probe (initially at a depth of 7 cm) in Test 3 was installed in order to monitor clogging effects in the shallow layer of the streambed. A total of five flood events were recorded and labeled as A to E, with stream water depths that fluctuated below 200 cm and streambed erosions of 2–19 cm (Figures 6a and 7a). Temperatures on the streambed surface (T00) and in the streambed at a depth of 50 cm (T50) were approximately 20–36°C during the period of investigation (Figure 6b).

[26] The depths of the probes varied as a result of the scour/fill of the streambed due to flooding. For example, in Test 2 the deeper probe was located at an initial depth of

Table 2. The Parameters for Heat Transfer Within a Streambed[a]

	Thermal Conductivity (W/m°C)	Density $\times 10^3$ (kg/m^3)	Specific Heat (kJ/kg°C)	Thermal Diffusivity $\times 10^{-7}$ (m^2/s)	References
Unconsolidated sand and gravel (saturated)	1.9	2.03	1.45	6.60	This Study
	2.5				*Farouki* [1981]
	2.08	1.65	1.70	7.50	*Lapham* [1989]
	2.3				*Ronan et al*. [1998]
	1.73–5.02				*Witte et al*. [2002]
	2.50	2.35			*Rohner et al*. [2005]
	3.6–4.2	1.5–1.7			*Markle et al*. [2006]
	1.4	1.99	2.09	3.36	*Keery et al*. [2007]
Unconsolidated sand and gravel(dry)	0.34	1.68	0.87	2.3	This Study
	0.4	1.6			*Farouki* [1981]
	0.77			4.5	*Austin et al*. [2000]
	0.7–0.9	1.75	0.86	4.6–6.0	*Chiasson et al*. [2000]
	0.7–0.9			5.7	*Gehlin et al*. [2003]
	0.83–1.04				*Witte et al*. [2002]
	0.47–0.51	1.9–2.1			*Naidu and Singh* [2004]
Quartzite	3–7	2.6–2.7	0.81–0.84	13–33	*Beardsmore and Cull* [2001]; *Clauser and Huenges* [1995]; *Jones* [2003]; *Sundberg et al*. [2005]
		2.1–2.5	0.83–0.88		This Study
Metasandstone	2–5	2.4–2.6			*Beardsmore and Cull* [2001]; *Clauser and Huenges* [1995]; *Jones* [2003]; *Sundberg et al*. [2005]
		2.1–2.4	0.81–0.87		This Study
Slate	4–7	2.6–2.9	0.88		*Beardsmore and Cull* [2001]; *Clauser and Huenges* [1995]; *Jones* [2003]; *Sundberg et al*. [2005]
		2.3–2.5	0.89–0.93		This Study
Quartz	7.7	2.6			*Beardsmore and Cull* [2001]; *Clauser and Huenges* [1995]; *Jones* [2003]; *Sundberg et al*. [2005]
Water	0.6	1.0	4.2	1.4	*Beardsmore and Cull* [2001]; *Clauser and Huenges* [1995]; *Jones* [2003]; *Sundberg et al*. [2005]
Air	0.026	0.0012	1.0	0.21	*Beardsmore and Cull* [2001]; *Clauser and Huenges* [1995]; *Jones* [2003]; *Sundberg et al*. [2005]

[a]Temperature and pressure at 25°C and 1 atm.

50 cm. Following Flood A, the top 4 cm of the streambed was eroded and the interval between the streambed surface and the deeper probe decreased to 46 cm. Noteworthy is that the streambed mainly experienced erosion during the investigation period, which may have contributed to the dam that served as a barrier to gravel in the upper reach, moving to the upper fan at our monitoring site.

[27] The pressures of the P50 were less than air pressures during the entire testing period of Tests 1 and 2, indicating that an unsaturated zone developed when the top of the streambed became clogged, and did not change to saturated during the three floods (Figure 6a). Following Floods A, B, and C the top 4, 2, and 4 cm of the streambed were eroded, respectively. The observation suggests that during a flood event an older clogged streambed may be eroded. However, a new one will quickly form to cause an unsaturated

Table 3. The Parameters for a Saturated and Unsaturated Streambed

	Saturated	Unsaturated			Dry
Water Content	0.35	0.25	0.15	0.05	0.00
Thermal Conductivity (W/m°C)	1.94	1.54	1.13	0.73	0.33
Density (kg/m^3)	2030	1970	1855	1738	1680
Specific Heat (J/kg°C)	1450	1300	1150	1000	850

Table 4. The Thermal Parameters for a Saturated Streambed With Different Percentages of Silt Fill-In

	Silt Fill-In (% Bulk Volume)			
	0	10	20	Slate-Quartzite
Porosity (%)	35	25	15	<5
Thermal Conductivity (W/m°C)	1.9	3.5	5.1	7.0
Density (kg/m^3)	2030	2176	2323	2600
Specific Heat (J/kg°C)	1450	1158	994	850

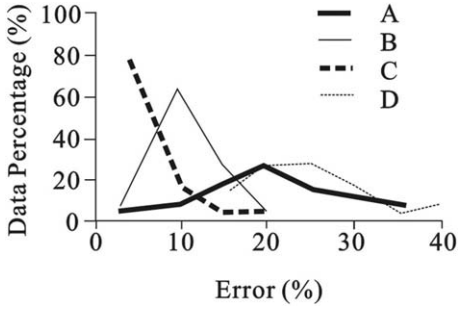

Figure 5. Errors from the uncertainties of the sensor spacing (a), streambed porosity (b), streambed thermal diffusivity (c), and temperature sensor accuracy (d) in this study.

zone to develop while the concentration of the suspended load in stream is high. Suspended loads in the stream were high, approximately 0.85 g/L in Flood B, with an average water depth of 30 cm and 6.53 g/L for an 80 cm water depth during Floods A and C (Figure 2). In floods with stream levels of 30–80 cm, stream flow has horizontal velocities of 0.5–1 m/s and more than 0.8 g/L of suspended sediment (~400 g/s/m^2). Several flume studies have indicated that sand infiltration (clogging) in the gravel bed reaches saturated in less than 1 h, while the fine sediment feed rate is >14 g/s/m^2 [*Wooster et al.*, 2008; *Gibson et al.*, 2011].

[28] During flood events in Tests 1 and 2, the infiltration rate did not linearly increase. Using the diurnal temperature cycles of T00 and T50, the infiltration rates were estimated with their depths adjusted for erosion and by assuming water contents of 0.25, 0.15, and 0.05, respectively (Figures 6b and c). The infiltration rates displayed a decreasing trend after the probe was buried; for example, from 1.25×10^{-5} to 3.5×10^{-6} m/s for an assumption of a water content of 0.15. The infiltration rates only increased suddenly in the beginning of the floods, then they decreased (in Floods A and C) or slightly fluctuated (in Flood B). An increase in the infiltration rate in the beginning of a flood indicates that the streambed was clogged in less than a short period of 2 days after an old clogging layer eroded (the resolution of the infiltration rate is 1 day).

[29] Pressure records within the streambed provided a more accurate timespan for the clogging processes. The pressure records of Test 3 indicated that the erosion of an old clogged layer and a new one were built only within an hour in Floods D and E (Figure 8). The pressure records of P50 during two flood events indicated a sudden increase in water depth with a 11–19 cm erosion of the streambed.

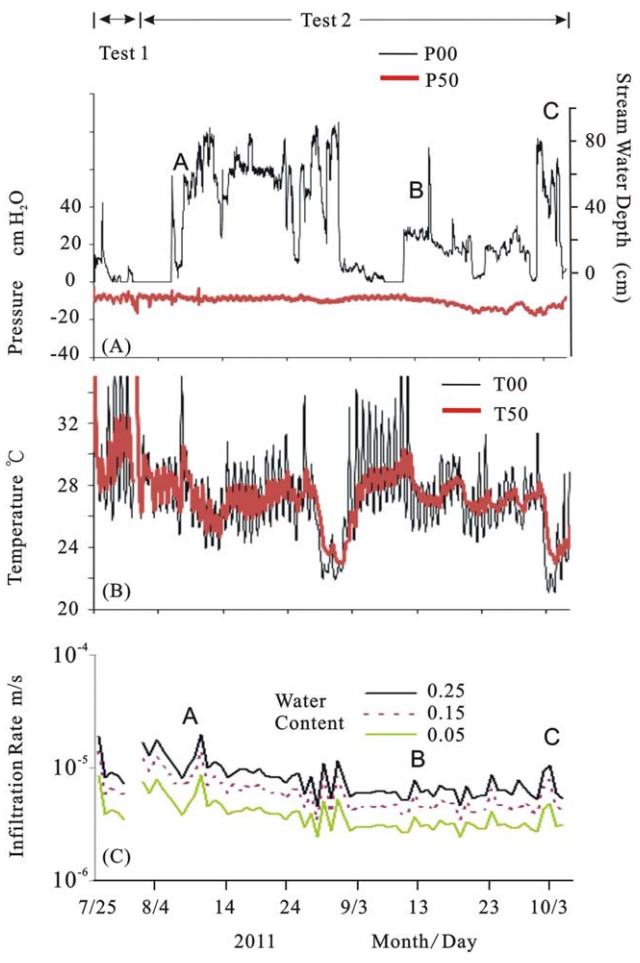

Figure 6. The data and the results from Tests 1 and 2. (a) Stream water depths (P00) and the pressures in the streambed (P50, initially at depth of 50 cm) with the air pressure subtracted. The letters A, B, and C represent flood events. (b) The temperature time series at an initial depth of 0 cm (T00) and 50 cm (T50). (c) The infiltration rates calculated from the temperature time series of T00-T50, assuming a water content of 0.25, 0.15, and 0.05.

Pressures were recorded over half hour intervals and there was only one point of pressure increase in the P50 in Figure 8a, indicating that the erosion of an old clogged layer and a new one had been built only within an hour. For Flood E, the stream water depth increased by approximately 140 cm while the 19 cm of the streambed was eroded. However, none of the pressure increases were recorded in P50 on 11 November when Flood E began (Figure 8b).

Table 5. The Test Date, Saturated Condition, Probe Depth, and Flood Events

	Date 2011	Condition	Probe Initial Depth (cm)	Flood Event: Scour/Fill[a] (cm)
Test 1	25 Jul to 2 Aug	Unsaturated	0-50	
Test 2	2 Aug to 5 Oct	Unsaturated	0-50	A (6 Aug): -4 B (11 Sep): -2 C (3 Oct): -4
Test 3	7 Oct to 19 Dec	Saturated-Unsaturated	0-7-50	D (26 Oct): -11 E (11 Nov): -19

[a]Symbol + for Fill; - for Scour.

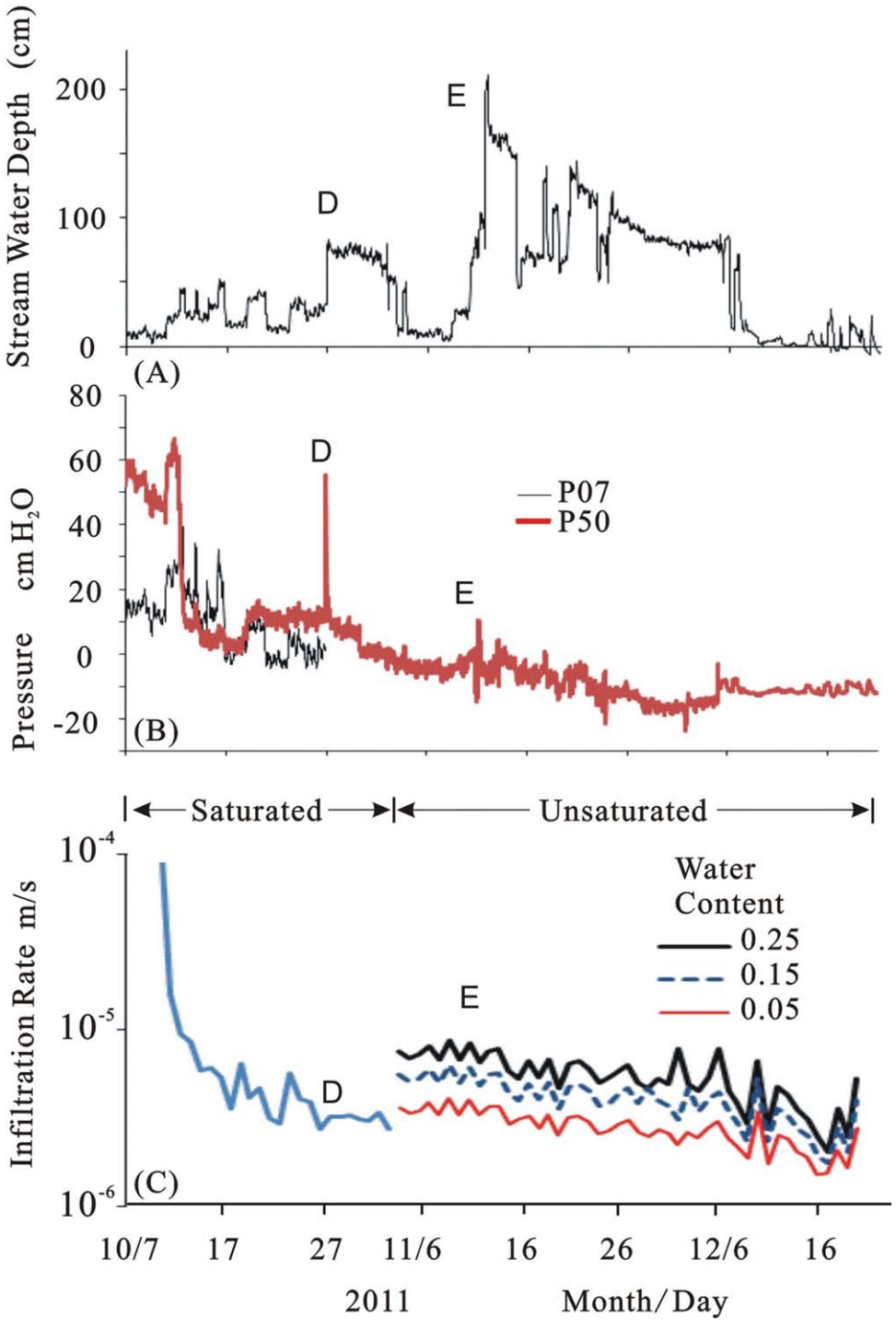

Figure 7. The data and the results from Test 3. (a) Stream water depths (P00). (b) The pressures of P07 and P50 with air pressure subtracted. An unsaturated zone developed on 3 November. The letters D and E denote flood events. (c) The infiltration rates determined from the temperature time series from T00-T50.

[30] Using temperature data for T00/T50, we estimated the infiltration rates for Test 3 (Figure 7c). The infiltration rates were very high ($>10^{-4}$ m/s) during the first few days when and after we dug and broke through the old clogged layer, the rates decreased to 2.8–5.3$\times 10^{-6}$ m/s (assuming a water content of 0.25–0.05) due to clogging. In another project during the same year, the infiltration rate was estimated using the water balance method (measuring river discharge), and an average infiltration rate of 4.2 $\times 10^{-6}$ m/s, identical to our values, was obtained [*Yao*, 2012]. Infiltration tests were conducted on the southern bank of the Choshui Stream, 3 km south of our test site during 1999–2000 [*Hsu and Huang*, 2003]. Stream water with sediment loads of approximately 0.2 g/L settled to form a 33 cm

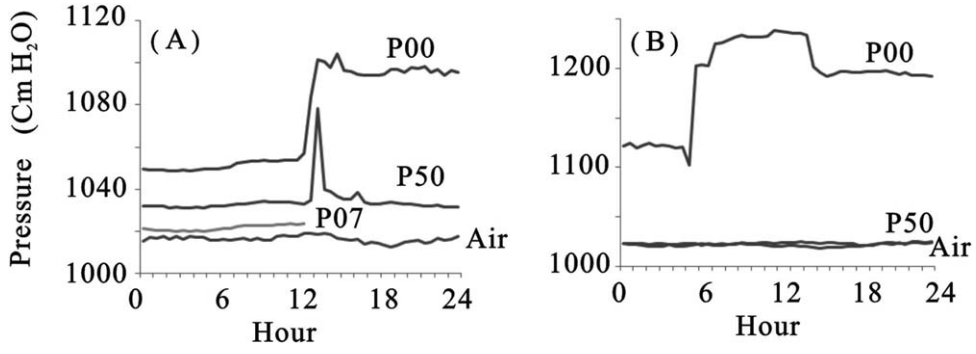

Figure 8. The air and streambed pressures of the two flood events (Floods D and E) recorded for a half-hour interval. The P00, P07, and P50 were at depths of 0, 7, and 50 cm, respectively. (a) In the beginning of Flood D, the stream water depth increased by approximately 50 cm and the streambed was eroded by 11 cm; but only one point of pressure in P50 changed for 26 October. (b) The stream water depth increased by 140 cm, the streambed eroded by 19 cm, and none of the pressure increased in P50 for 11 November for Flood E.

thick sandy mud clogging layer on the streambed surface during the 2 months, reducing the pond infiltration rate to 9.8×10^{-6} m/s. The hydraulic conductivities of the clogging layer were determined to be approximately 3.8×10^{-6} to 1.7×10^{-7} m/s. The infiltration rate and the hydraulic conductivity were similar to our results.

[31] Higher stream water levels during Floods D and E (Figure 7a) did not linearly increase P50 pressures (Figure 7b) and infiltration rates (Figure 7c). According to Darcy's law, the velocity should increase linearly with an increased pressure head gradient while the hydraulic conductivity remains constant. However, our field data indicated that the hydraulic conductivities were not constant. In an actual river, in this case a disconnected gravel stream, clogging of the clogged layer was considered. Our study suggests that stream flow with a high turbidity can cause clogging on/in the streambed and can very quickly reduce the percolation velocity and the hydraulic conductivity. Even during a low-level period (0–30 cm), suspended sediment loads of 0.02–1.0 g/L (sediment rates 8–25 g/s/m^2) exist (Figure 2). For some no flow days, we observed mud/silt drapes of 0.1–1 cm thick deposited on the streambed.

5.2. Clogging and Preferential Flow

[32] Three probes at 0–7-50 cm in depth in the streambed were installed in Test 3 in order to evaluate clogging processes in shallow and deeper layers. The three probes were all located within a saturated condition during the early days of Test 3, and during the low-level and lower sediment load period prior to Flood D (Figure 7). As demonstrated by the pressures of the P50 less than ambient air pressures, an unsaturated zone developed after 3 November. Hydraulic gradients within the shallow layer (0–7 cm) displayed an increasing trend from 0.24 to 5.88, with variations caused by clogging and stream water level fluctuations (Figure 9a). Percolation velocities within the shallow layer also displayed a decreasing trend from 10^{-3} to 10^{-5} m/s. We suggest that they were also caused by continuous clogging (Figure 9b).

[33] The variation of vertical hydraulic conductivity of the two layers indicate that clogging initially developed within the 0–50 cm of the streambed, but lastly only in the shallow layer (0–7 cm). Vertical hydraulic conductivities were calculated as the percolation velocity divided by the vertical hydraulic gradient. In the last half of the data, the hydraulic conductivities of the shallow layer (0–7 cm) were approximately $2.6–5.5\times10^{-6}$ m/s, an order of magnitude lower than the values of the deeper layer (7–50 cm), $3.1–5.4\times10^{-5}$ m/s (Figure 9b). The average vertical hydraulic conductivity of the shallow layer within the last half of the

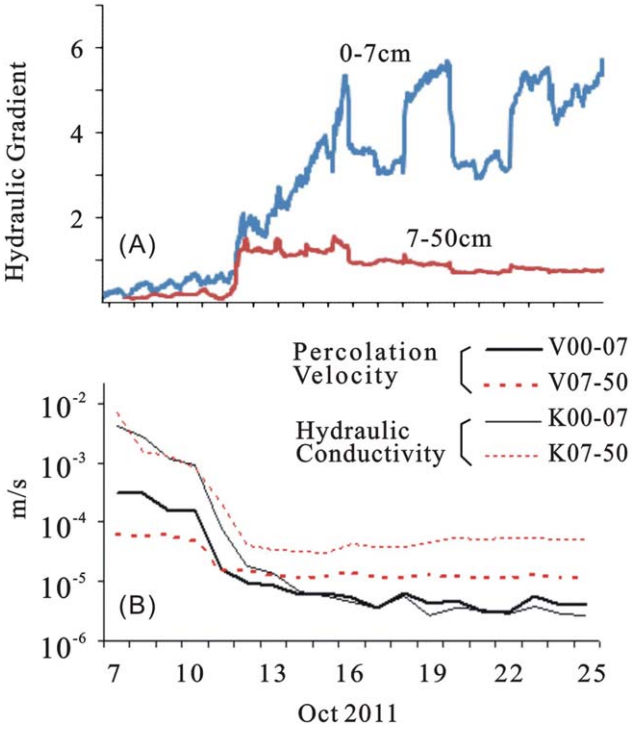

Figure 9. The hydraulic gradient, the percolation velocity, and the hydraulic conductivity in the two layers. (a) The hydraulic gradients in the shallow layer (between depths of 0–7 cm) and the deeper layer (7–50 cm). (b) The percolation velocity V00–07 for the shallow layer, V07–50 for the deeper layer, hydraulic conductivities K00–07 for the shallow layer, and K07–50 for the deeper layer.

data was approximately 4.1×10^{-6} m/s, 100 to 1000 times smaller than the values of 10^{-3} to 10^{-4} m/s as determined from the pumping tests of monitoring wells [*Central Geological Survey*, 1999].

[34] According to the data of Test 3, the thickness of the clogging layer at our study site was more than 7 cm and less than 50 cm. The thickness of the clogging layer in the sand/gravel streambed is determined by varied conditions of particle size, discharge, velocity, slope and rates of sediment transport. However, in a variety of studies conducted in flumes and natural rivers, the range of the thickness is only a few centimeters [*Beschta and Jackson*, 1979; *Blaschke et al*., 2003; *Wooster et al*., 2008; *Gibson et al*., 2011].

[35] After a clogging layer develops, preferential flow must be formed in the deeper layer. Considering percolation in a two layer system for the conservation of mass, the following equation is employed:

$$v_1A_1=v_2A_2 \tag{4}$$

where v_1 and v_2 are the percolation velocities for the shallow and deeper layer, and A_1 and A_2 are the horizontal cross-sectional areas for the saturated percolation flow in each layer (Figure 10). Ratios of v_1/v_2 greater than 1, at the beginning of Test 3 (7–11 October), can be explained as those that occur when the clogged layer is removed during the installation of sensors. For such a case, percolation flow occurred not only vertically but horizontally, and passed through a larger cross section in the once unsaturated zone (Figures 10a and 11). During this period, the percolation velocity within the surface region with reduced resistance (not yet clogged) of the shallow layer was greater than the velocity within the deeper layer. After the reduced resistance region is clogged to the degree that the hydraulic conductivity of the shallow layer is less than the deeper layer, a preferential flow with a smaller cross section must be formed within the deeper layer with $v_1 < v_2$ (Figure 10b) [*Glass et al*., 1989; *Hendrickx and Flury*, 2001].

5.3. Compression of the Clogging Layer

[36] An increase in stream stage will increase the hydraulic gradient and the downward drag force within the clogged layer, and compresses its matrix of silt and clay [*Houston et al*., 1999]. The hydraulic conductivities of the upper 7 cm clogged layer in Figure 9b were approximately $10^{-5}-10^{-6}$ m/s, indicating silt composition [*Shepherd*, 1989]. Additionally, the sand fraction accounted for 33% of total streambed sediments (Figure 3a), leaving only voids that silt and clay could infiltrate. The matrix (<0.12 mm grain size) of the upper 10 cm streambed at our site was collected and its grain size distribution is shown in Figure 12a. The matrix is composed mainly of silt (62%) with very fine sand (20%) and clay (18%). For the lower effective stress loading from 1 to 40 kPa, approximately 0.1–4 m of water pressure, the compression index (Ci) for the matrix is 0.04 (Figure 12b).

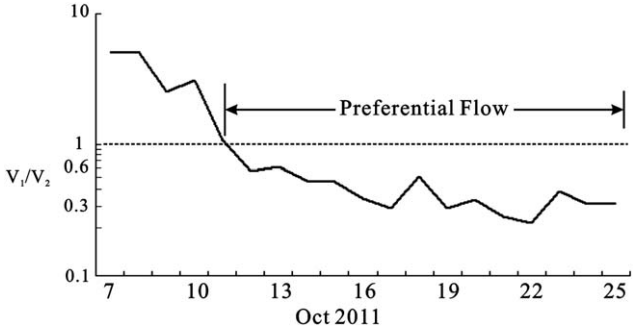

Figure 11. The percolation velocity ratio v_1/v_2 during the period of 7–25 October 2011.

[37] A Ci of 0.04 implies an increase of 1 order of magnitude in pressure (e.g., the stream water depth from 0.1 to 1 m) within the silt clogged layer, the void ratio (e) will decrease by 0.04. According to the Kozeny-Carman equation [*Spencer*, 1968; *Solanki*, 2012; *Widodo and Ibrahim*, 2012], as follows:

$$K=C\times1/S^2\times e^3/(1-e)^2 \tag{5}$$

where K is the hydraulic conductivity (m/s), C is a constant (assuming a value of 1/180), S is the specific surface (m^2/kg), and e is the void ratio. Assuming that clogging silt is spherical in shape with a grain size of 10^{-5}m, S is

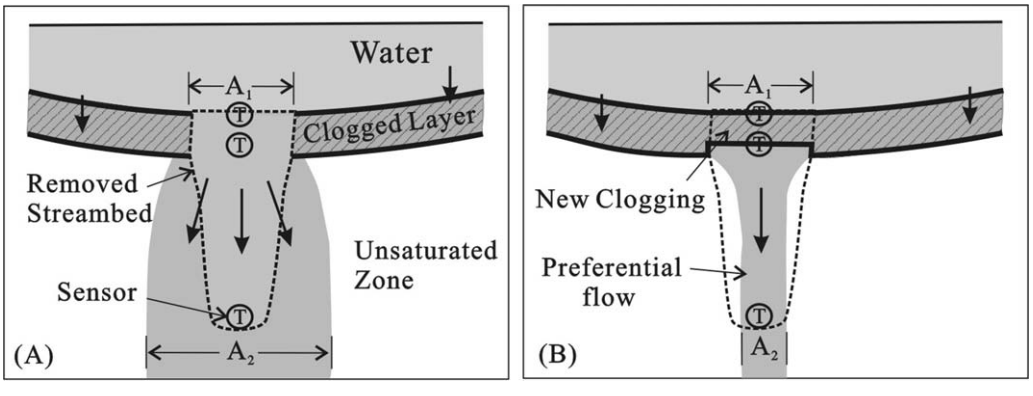

Figure 10. The explanation for the percolation velocity ratio, v_1/v_2. (a) The ratio of v_1/v_2 was greater than 1 before a new clogging layer formed. (b) The ratio of v_1/v_2 was less than 1 after a new clogging layer formed.

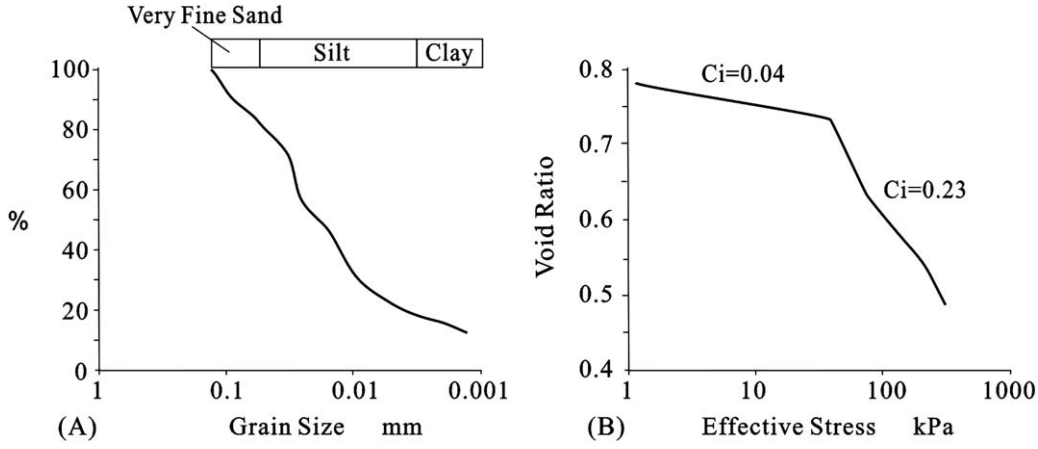

Figure 12. (a) The grain size distribution of the upper 10 cm streambed matrix. (b) The compression index (Ci) for the matrix. The Ci value is lower for a lower effective stress (<40 kPa).

120 m^2/kg, e is 0.80 (porosity 0.44), and K is 5.06×10^{-6} m/s. Increasing one order of water depth, the silt clogged layer may decrease its void ratio to 0.76 and the hydraulic conductivity may decrease to 2.96×10^{-6} m/s, nearly half.

6. Discussion

[38] The infiltration rates in a clay clogged pond and in a paddy field were approximately 10^{-8} m/s [*Lin et al*., 1998; *Chen et al*., 1998], as compared to our infiltration rates of approximately 10^{-6} m/s for a silt clogged gravel stream. A coarse sediment deposit is defined as saturated with fine sediment when the pore spaces of the deposit become so small that fine sediment can no longer advance; for example, sand infiltrates into gravel interstices. However, finer sediment (e.g., silt or clay) can infiltrate a gravel bed previously saturated with sand. For our case, during the end of Tests 2 and 3, the clogged streambed was likely saturated with sand and silt, but not with clay. The downward movement of sand and silt particles was only driven by gravity, infiltrating into interstices of the top several centimeters [*Wooster et al*., 2008]. However, for cases of clay infiltration downward movement could be driven by a combination of gravity and intrasand flow. If clay goes down to the deeper unsaturated zone, passing the silt clogged layer beneath the streambed, then it is not easily saturated with clay within a short period of time.

[39] Many examples of clogging streambeds can be found in natural rivers [*Schalchli*, 1992; *Treese et al*., 2007; *Brunner et al*., 2009]. Due to clogging, infiltration rates in the Rhine River near Flehe with a Quaternary gravel streambed were reduced to approximately 1.1×10^{-5} m/s [*Schubert*, 2006]. Infiltration rates in Fowlers Creek in Australia were as low as 10^{-6} to 10^{-7} m/s due to clogging [*Dunkerley*, 2008]. For the Vicee Canyon in Nevada, *Ronan et al*. [1998] did not mention clogging in their work, but did suggest a lower hydraulic conductivity surface layer in the simulation model; and assigned a saturated hydraulic conductivity value of 1.75×10^{-6} m/s for the upper 3 mm streambed surface as compared to 7.0×10^{-5} m/s for underlying sediments. We suggest that the clogging phenomenon is common, rather than a special case, for deep groundwater table streams.

[40] The flashy ephemeral streams in semiarid and arid regions of the American Southwest are excellent examples for understanding flooding streambed infiltration in disconnected streams [*Stonestrom et al*., 2007]. The recharge of groundwater was essentially due to flood events, and streambed infiltration during flood events experienced clogging. A smaller saturated hydraulic conductivity, 2.4×10^{-5} m/s, was assigned to the upper streambed, while a larger value of 7.0×10^{-3} m/s was assigned to the deeper layer in a numerical simulation for Arroyo Hondo, New Mexico [*Moore*, 2007]. *Constantz et al*. [2002] reported an initial streambed infiltration rate of 2.3×10^{-5} m/s within the Santa Fe River, followed by a steady streambed infiltration rate of 1.1×10^{-6} m/s. We suggest that the factors affecting the infiltration rate of water in a disconnected stream should include continuous clogging (a decrease of hydraulic conductivity within the clogging layer) and compression of the clogged layer while increasing the water depth.

7. Conclusions

[41] A disconnected stream is formed by a deep groundwater table and clogging in the upper part of the streambed. In general, for highly suspended sediments in stream water, the time needed to saturate a clogged layer with silt is shorter. An old, clogged layer may be removed, but since the suspended load is highest during a flood a new one is quickly formed. In this work, we have presented new pressure and infiltration data for a disconnected stream over a period of 167 days for five flood events. Our data did not support the theory that flooding linearly increases the infiltration rate. Infiltration rates were also low during the flooding season. For water infiltration simulations in a streambed for a disconnected stream, we suggest that the degree of clogging and scour/sedimentation and compression of a clogged layer during the flooding period should be considered. However, the total recharge amount to the aquifer will be increased as a result of the increase of the wet perimeter in the stream during the flood period.

[42] **Acknowledgments.** We thank the Central Geological Survey of Taiwan for financial support and Professors C. H. Lee, K. C. Hsu, three reviewers, and editors for helpful comments and suggestions.

References

Anderson, M. P. (2005), Heat as a ground water tracer, *Ground Water*, *43*, 951–968, doi:10.1111/j.1745-6584.2005.00052.x.

Austin, W., C. Yavuzturk, and J. D. Spitler (2000), Development of an in-situ system for measuring ground thermal properties, *ASHRAE Trans.*, *106*(1), 365–379.

Beardsmore, G. R., and J. P. Cull (2001), *Crustal Heat Flow*, Cambridge Univ. Press, Cambridge, U. K.

Behnke, J. J. (1969), Clogging in surface spreading operation for artificial ground-water recharge, *Water Resour. Res.*, *5*, 870–876, doi:10.1029/WR005i004p00870.

Beschta, R. L., and W. L. Jackson (1979), The intrusion of fine sediments into a stable gravel bed, *J. Fish. Res. Board Can.*, *36*, 204–210, doi:10.1139/f79-030.

Blaschke, A. P., K. H. Steiner, R. Schmalfuss, D. Gutknecht, and D. Sengschmitt (2003), Clogging processes in hyporheic interstices of an impounded river, the Danube at Vienna, Austria, *Int. Rev. Hydrobiol.*, *88*, 397–413, doi:10.1002/iroh.200390034.

Bouwer, H. (2002), Artificial recharge of groundwater: Hydrogeology and engineering, *Hydrogeology J.*, *10*, 121–142, doi:10.1007/s10040-001-0182-4.

Bouwer, H., and R. C. Rice (1989), Effect of water depth in groundwater recharge basins on infiltration, *J. Irrig. Drain. Eng.*, *115*, 556–567, doi:10.1061/(ASCE)0733-9437(1989)115:4(556).

Brunner, P., P. G. Cook, and C. T. Simmons (2009), Hydrogeologic controls on disconnection between surface water and groundwater, *Water Resour. Res.*, *45*, W01422, doi:10.1029/2008WR006953.

Brunner, P., P. G. Cook, and C. T. Simmons (2011), Disconnected surface water and groundwater: From theory to practice, *Ground Water*, *49*, 460–467, doi:10.1111/j.1745-6584.2010.00752.x.

Central Geological Survey (1999), *The Hydrogeological Investigation Report of the Choshuishi Alluvial Fan* [in Chinese], Taipei.

Chang, J. C. (1983), A review of channel shift on Choshui alluvial fan [in Chinese], *Geogr. Res.*, *7*, 85–92.

Chen, S. K., C. W. Liu, and W. C. Huang (1998), Experimental study the hydraulic characteristics of infiltration in paddy field [in Chinese], *J. Taiwan Water Conserv.*, *46*(4), 52–65.

Chen, W. F., and T. K. Liu (2003), Dissolved oxygen and nitrate of groundwater in Choshui fan-delta, Western Taiwan, *Environ. Geol.*, *44*, 731–737, doi:10.1007/s00254-003-0823-0.

Chen, W. F., and T. K. Liu (2005), Ion activity products of iron sulfides in groundwater, *Geochim. Cosmochim. Acta*, *69*, 3535–3544, doi:10.1016/j.gca.2005.03.007.

Chiasson, A. C., S. J. Rees, and J. D. Spitler (2000), A preliminary assessment of the effects of ground-water flow on closed-loop ground-source heat pump systems, *ASHRAE Trans.*, *106*(1), 380–393.

Clauser, C., and E. Huenges (1995), Thermal conductivity of rocks and minerals, in *Rock Physics and Phase Relations – A Handbook of Physical Constants*, vol. *3*, edited by T. J. Ahrens, pp. 105–126, AGU, Washington, D. C. doi:10.1029/RF003p0105.

Constantz, J. (2008), Heat as a tracer to determine streambed water exchanges, *Water Resour. Res.*, *44*, W00D10, doi:10.1029/2008WR006996.

Constantz, J., A. E. Stewart, R. Niswonger, and L. Sarma (2002) Analysis of temperature profiles for investigating stream losses beneath ephemeral channels, *Water Resour. Res.*, *38*(12), 1316, doi:10.1029/2001WR001221.

Dahan, O., B. Tatrsky, Y. Enzel, C. Kulls, M. Seely, and G. Benito (2008), Dynamics of flood-water infiltration and ground-water recharge in hyperarid desert, *Ground Water*, *46*, 450–461, doi:10.1111/j.1745-6584.2007.00414.x.

Desilets, S. L. E., T. P. A. Ferre, and P. A. Troch (2008), Effects of stream-aquifer disconnection on local flow patterns, *Water Resour. Res.*, *44*, W09501, doi:10.1029/2007WR006782.

Doble, R. C., R. S. Crosbie, B. D. Smerdon, L. Peeters, and F. J. Cook (2012), Groundwater recharge from overbank floods, *Water Resour. Res.*, *48*, W09522, doi:10.1029/2011WR011441.

Dunkerley, D. L. (2008), Bank permeability in an Australian ephemeral dry-land stream: Variation with stage resulting from mud deposition and sediment clogging, *Earth Surf. Processes Landforms*, *33*(2), 226–243, doi:10.1002/esp.1539.

Farouki, O. T. (1981), Thermal properties of soils, *CRREL Monogr. 81-1*, 151 pp., United States Corps of Engineers, Hanover, N. H., doi:10.1016/0165-232X(81)90041-0.

Gehlin, S., G. Helstrom, and B. Nordell (2003), The influence of the thermosiphon effect on the thermal response, *Renewable Energy*, *28*(14), 2239–2254, doi:10.1016/S0960-1481(03)00129-0.

Gibson, S., R. Heath, D. Abraham, and D. Schoellhamer (2011), Visualization and analysis of temporal trends of sand infiltration into a gravel bed, *Water Resour. Res.*, *47*, W12601, doi:10.1029/2011WR10486.

Glass, R. J., T. S. Steenhuis, and J. Y. Parlange (1989), Wetting front instability: 2. Experimental determination of relationships between system parameters and two-dimensional unstable flow field behavior in initially dry porous media, *Water Resour. Res.*, *25*, 1195–1207, doi:10.1029/WR025i006p01195.

Hatch, C. E., A. T. Fisher, J. S. Revenaugh, J. Constantz, and C. Ruehl (2006), Quantifying surface water/ground water interactions using time series analysis of streambed thermal records: Method development, *Water Resour. Res.*, *42*, W10410, doi:10.1029/2005WR004787.

Hatch, C. E., A. T. Fisher, C. R. Ruehl, and G. Stemler (2010), Spatial and temporal variations in streambed hydraulic conductivity quantified with time-series thermal methods, *J. Hydrol.*, *389*, 276–288, doi:10.1016/j.jhydrol.2010.05.046.

Heath, D. L. (1983), Flood and recharge relationships of the lower Rio Puerco New Mexico, MS thesis, Dep. of Geol., N. M. Inst. of Min. and Technol, Socorro, N. M.

Hendrickx, J. M. H., and M. Flury (2001), Uniform and preferential flow mechanisms in the vadose zone, in *Conceptual Models of Flow and Transport in the Fractured Vadose Zone*, edited by National Research Council, pp. 149–187, Natl. Acad. Press, Washington, D. C.

Houston, S. L., P. D. Duryea, and R. Hong (1999), Infiltration considerations for groundwater recharge with waste effluent, *J. Irrig. Drain. Eng.*, *125*, 264–272, doi:10.1061/(ASCE)0733-9437(1999)125:5(264).

Hsu, S. M., and W. Q. Huang (2003), Simulation and investigation of clogging phenomena in an artificial recharge pond [in Chinese], *J. Taiwan Water Conserv.*, *51*, 53–62.

Irvine, D. J., P. Brunner, H. H. Franssen, and C. T. Simmons (2012), Heterogeneous or homogeneous? Implications of simplifying heterogeneous streambeds in models of losing streams, *J. Hydrol.*, *424-425*, 16–23, doi:10.1016/j.jhydrol.2011.11.051.

Jones, M. Q. W. (2003), Thermal properties of stratified rocks from Witwatersrand gold mining areas, *J. S. Afr. Inst. Min. Metall.*, *103*(3), 173–186.

Keery, J., A. Binley, N. Crook, and J. W. N. Smith (2007), Temporal and spatial variability of groundwater-surface water fluxes: Development and application of an analytical method using temperature time series, *J. Hydrol.*, *336*, doi:10.1016/j.jhydrol.2006.12.003.

Kukkonen, I., L. Kivekas, S. Vuoriainen, and M. Kaaria (2011), Thermal properties of rocks in Olkiluoto: Results of laboratory measurements, *Geol. Surv. of Finland Working Rep. 2011-17*, Geological Survey of Finland, Espoo, Finland.

Lapham, W. W. (1989), Use of temperature profiles beneath streams to determine rates of vertical groundwater flow and vertical hydraulic conductivity, *U.S. Geol. Surv. Water Supply Pap. 2337*, 35 pp.

Lentz, R. D., and L. L. Freeborn (2007), Sediment and polyacrylamide effects on seepage from channeled flows, *Soil Sci.*, *172*, 770–789, doi:10.1097/ss.0b013e3180de4a33.

Lin, J. C., C. H. Chen, Y. C. Tan (1998), Experiments and simulations of infiltration recharge of a storage pond [in Chinese], *J. Chin. Agric. Eng.*, *44*(4), 24–36.

Markle, J. M., R. A. Schincariol, J. H. Sass, and J. M. Molson (2006), Characterizing the two-dimensional thermal conductivity distribution in a sand and gravel aquifer, *Soil Sci. Soc. Am. J.*, *70*, 1281–1294, doi:10.2136/sssaj2005.0293.

Massmann, J., and D. F. Farrier (1992), Effects of atmospheric pressures on gas transport in the vadose zone, *Water Resour. Res.*, *28*, 777–791, doi:10.1029/91WR02766.

McDonald, M. G., and A. W. Harbaugh (1996), A modular three-dimensional finite difference groundwater model, in *Techniques of Water-Resources Investigations*, Book 6, chap. A1, U. S. Geol. Surv., Denver, Colo.

Moore, J. E., and C. T. Jenkins (1966), An evaluation of the effect of groundwater pumpage on the infiltration rate of a semipervious streambed, *Water Resour. Res.*, *2*, 691–696, doi:10.1029/WR002i004p00691.

Moore, S. J. (2007), Streamflow, infiltration, and recharge in Arroyo Hondo, New Mexico, in *Ground-Water Recharge in the Arid and Semiarid Southwestern United States*, edited by D. A. Stonestrom et al., U.S. Geol. Surv. Prof. Pap. 1703, pp. 137–156, U. S. Geol. Surv., Denver, Colo.

Munz, M., S. E. Oswald, and C. Schmidt (2011), Sand box experiments to evaluate the influence of subsurface temperature probe design on temperature based water flux calculation, *Hydrol. Earth Syst. Sci.*, *15*, 3495–3510, doi:10.5194/hess-15-3495-2011.

Naidu, A. D., and D. N. Singh (2004), A generalized procedure for determining thermal resistivity of soils, *Int. J. Therm. Sci.*, *43*, 43–51, doi:10.1016/S1290-0729(03)00103-O.

Neeper, D. A. (2002), Investigation of the vadose zone using barometric pressure cycles, *J. Contam. Hydrol.*, *54*, 59–80, doi:10.1016/S0169-7722(01)00146-2.

Niswonger, R., and D. E. Prudic (2003), Modeling heat as a tracer to estimate streambed seepage and hydraulic conductivity, *U.S. Geol. Surv. Circ. 1260*, pp. 81–89, U. S. Geol. Surv., Denver, Colo.

Osman, Y. Z., and M. P. Bruen (2002), Modelling stream-aquifer seepage in an alluvial aquifer: An improved loosing-stream package for MODFLOW, *J. Hydrol.*, *264*, 69–86, doi:10.1016/S0022-1694(02)00067-7.

Parsons, S., R. Evans, and M. Hoban (2008), Surface-groundwater connectivity assessment, in *A Report to the Australian Government From the CSIRO Murray-Darling Basin Sustainable Yields Project 35*, Commonw. Sci. and Ind. Res. Organ., Clayton, Vic.

Pavelic, P., P. J. Dillon, M. Mucha, T. Nakai, K. E. Barry, and E. Bestland (2011), Laboratory assessment of factors affecting soil clogging of soil aquifer treatment systems, *Water Res.*, *45*, 3153–3163, doi:10.1016/j.watres.2011.03.027.

Peterson, D. M., R. Khaleel, and J. W. Hawley (1984), Quasi three-dimensional modeling of groundwater flow in the Mesilla Bolson, New Mexico and Texas, *N. M. Water Resour. Res. Inst. Proj. 1–3-45645*, N. M. Water Resour. Res. Inst, Las Cruces, N. M.

Rohner, E., L. Rybach, and U. Scharli (2005), A new, small, wireless instrument to determine ground thermal conductivity in-situ for borehole heat exchanger design, paper presented at World Geothermal Congress 2005, Antalya, Turkey, International Geothermal Association.

Ronan, A. D., D. E. Prudic, C. E. Thodal, and J. Constantz (1998), Field study and simulation of diurnal temperature effects on infiltration and variably saturated flow beneath an ephemeral stream, *Water Resour. Res.*, *34*, 2137–2153, doi:10.1029/98WR01572.

Scanlon, B. R., R. W. Healy, and P. G. Cook (2002), Choosing appropriate techniques for quantifying groundwater recharge, *Hydrogeol. J.*, *10*, 18–39, doi:10.1007/s10040-001-0176-2.

Schalchli, U. (1992), The clogging of coarse gravel river beds by fine sediment, *Hydrobiologia*, *235/236*, 189–197, doi:10.1007/BF00026211.

Schalchli, U. (1995), Basic equations for siltation of riverbeds, *J. Hydraul. Eng.*, *121*, 274–287, doi:10.1061/(ASCE)0733-9429(1995)121:3(274).

Schubert, J. (2006), Experience with Riverbed Clogging Along the Rhine River, in *Riverbank Filtration Hydrology,* edited by S. A. Hubbs*, NATO Science Series IV: Earth and Environmental Sciences*, pp. 221–242, Springer, Netherlands, doi:10.1007/978-1-4020-3938-6_10.

Shanafield, M., C. Hatch, and G. Pohll (2011), Uncertainty in thermal time series analysis estimates of streambed water flux, *Water Resour. Res.*, *47*, W03504, doi:10.1029/2010WR009574.

Shanafield, M., P. G. G. Cook, P. Brunner, J. L. McCallum, and C. T. Simmons (2012), Aquifer response to surface water transience in disconnected streams, *Water Resour. Res.*, *48*, W11510, doi:10.1029/2012WR012103.

Shepherd, R. G. (1989), Correlations of permeability and grain size, *Ground Water*, *27*, 633–638, doi:10.1111/j.1745-6584.1989.tb00476.x.

Silliman, S. E., and D. F. Booth, (1993), Analysis of time-series measurements of sediment temperature for identification of gaining vs. losing portions of Judy Creek, Indiana, *J. Hydrol.*, *146*, 131–148, doi:10.1016/0022-1694(93)90273-C.

Silliman, S. E., J. Ramirez, and R. L. McCabe (1995), Quantifying downflow through creek sediments using temperature time series: One One-dimensional solution incorporating measured surface temperature, *J. Hydrol.*, *167*, 99–119, doi:10.1016/0022-1694(94)02613-G.

Simpson, S. C., and T. Meixner (2012) Modeling effects of floods on streambed hydraulic conductivity and groundwater-surface water interactions, *Water Resour. Res.*, *48*, W02515, doi:10.1029/2011WR011022.

Solanki, C. H. (2012), Quick computation of settlement for shallow foundations of alluvial deposits, paper presented at International Conference on Chemical, Civil and Environment Engineering, Planetary Scientific Research Centre, Dubai.

Sophocleous, M. (2002), Interactions between groundwater and surface water: The state of the science, *Hydrogeol. J.*, *10*, 52–67, doi: 10.1007/s10040-001-0170-8.

Soto-Lopez, C. D., T. Meixner, and T. P. A. Ferre (2011) Effects of measurement resolution on the analysis of temperature time series for stream-aquifer flux estimation, *Water Resour. Res.*, *47*, W12602, doi:10.1029/2011WR010834.

Spencer, J. I. (1968), The influence of silt on the compressibility of an illitic clay, MS thesis, Dep. of Geol., Univ. of Missouri, Rolla.

Stallman, R. W. (1965), Steady one-dimensional fluid flow in a semi-infinite porous medium with sinusoidal surface temperature, *J. Geophys. Res.*, *70*, 2821–2827, doi:10.1029/JZ070i012p02821.

Stonestrom, D. A., and K. W. Blasch (2003), Determining temperature and thermal properties for heat-based studies of surface-water ground-water interactions, in *Heat as a Tool for Studying the Movement of Ground Water Near Streams*, edited by D. A. Stonestrom and J. Constantz *U.S. Geol. Surv. Circ. 1260*, pp. 73–80, U. S. Geol. Surv., Reston, Va.

Stonestrom, D. A., and J. Constantz (2003), Heat as a tool for studying the movement of ground water nears streams, *U.S. Geol. Surv. Circ. 1260*, 96 pp.

Stonestrom, D. A., J. Constantz, T. P. A. Ferre, and S. A. Leake (2007), Ground-Water Recharge in the arid and semiarid southwestern United States, *U.S. Geol. Surv. Prof. Pap. 1703*, 1–426.

Su, G. W., J. Jasperse, D. Seymour, J. Constantz, and Q. Zhou (2007), Analysis of pumping-induced unsaturated regions beneath a perennial river, *Water Resour. Res.*, *43*, W08421, doi:10.1029/2006WR005389.

Sundberg, J. S., P. E. Back, and G. Hellstrom (2005), Scale dependence and estimation of rock thermal conductivity, *SKB Rep. R-05-82*, Swed. Nucl. Fuel and Waste Manage. Co., Stockholm.

Suzuki, S. (1960), Percolation measurements based on heat flow through soil with special reference to paddy fields, *J. Geophys. Res.*, *65*, 2883–2885, doi:10.1029/JZ065i009p02883.

Treese, S., T. Meixner, J. Hogan, and A. McCoy (2007), Artificial streams, distorted processes: The effect of effluent on stream-aquifer interactions, *Eos Trans. AGU*, *88*(52), Fall Meet. Suppl., Abstract H24F-06.

Tsai, T. C., C. C. Wu, and W. R. Hsu, (2008), On soil temperature analyses and soil thermal diffusivity estimation in Taiwan [in Chinese], *Atmos. Sci.*, *36*, 83–100.

Vazquez-Sune, E., B. Capino, E. Abarca, and J. Carrera, (2007) Estimation of recharge from floods in disconnected stream-aquifer systems, *Ground Water*, *45*, 579–589, doi:10.1111/j.1745-6584.2007.00326.x.

Widodo, S., and A. Ibrahim (2012), Estimation of primary compression index using physical properties of Pontianak soft clay, *Int. J. Eng. Res. Appl.*, *2*(5), 2232–2236.

Witte, H. J. L., G. J. Gelder, and J. D. Spitler (2002), In situ measurement of ground thermal conductivity: A Dutch perspective, *ASHRAE Trans.*, *108*, 4521–4532.

Wooster, J. K., S. R. Dusterhoff, Y. Cui, L. S. Sklar, W. E. Djetrich, and M. Malko (2008), Sediment supply and relative size distribution effects on fine sediment infiltration into immobile gravels, *Water Resour. Res.*, *44*, W03424, doi:10.1029/2006WR005815.

Yao, C. Y. (2012), An introduction to the recharge project in the Choshui stream [in Chinese], in *Information on Land Subsidence*, edited by C. Y. Yao, pp. 1–9, Water Resour. Agency, Taipei.